TRPM4 promotes ErSO-mediated oncosis-like cell death in prostate cancer cells

Yuka Hoshi-Kadonosawa [1,2], Daiki Taniyama[1,3], William C. Reinhold[1*], Naoko Takebe[1,4*], Yves Pommier[1*]

[1] Developmental Therapeutics Branch, Center for Cancer Research, National Cancer Institute, National Institutes of Health, Bethesda, MD, USA

[2] Department of Obstetrics and Gynecology, Hirosaki University Graduate School of Medicine, Hirosaki, Aomori, Japan.

[3] Department of Molecular Pathology, Graduate School of Biomedical and Health Sciences, Hiroshima University, Hiroshima, Japan.

[4] Wilmot Cancer Institute, University of Rochester, School of Medicine and Dentistry, Rochester, NY, USA

* Corresponding authors

Running Title: TRPM4 Promotes ErSO-mediated Oncosis in Prostate Cancer

Keywords: TRPM4, ErSO, Drug Repurposing, Prostate Cancer, Oncosis, Cell Swelling, Biomarker, Therapeutics

Corresponding Authors

Yves Pommier and William Reinhold, Developmental Therapeutics Branch, CCR/NCI, NIH. Building 37, Room 5068 Bethesda, MD 20892-4255, USA, Phone: 240-760-6142, E-mail: pommier@nih.gov

Naoko Takebe, Wilmot Cancer Institute, University of Rochester, School of Medicine and Dentistry, Department of Medicine, Division of Hematology Oncology
601 Elmwood Avenue, Box704, Rochester, NY 14642, USA
Phone: 585-275-5830
Email: naoko_takebe@urmc.rochester.edu / Takeben@gmail.com

Conflict of Interest

N. Takebe reports serving as a consultant or advisor for ATX, CorriXR Therapeutics, and FRONTEO. Y. Pommier reports serving as a consultant for Sutro, PharmaMar, and Amgen and as Co-Chair of the Research Council of the Bloom Syndrome Association. No disclosures were reported by the other authors.

Downloaded from aacrjournals.org/cancerrescommun/article-pdf/doi/10.1158/2767-9764.CRC-26-0215/3840575/crc-26-0215.pdf by National Institutes of Health user on 31 October 2026

Abstract

Advanced and treatment-refractory prostate cancer remains a major clinical challenge and requires new therapeutic strategies. The calcium-activated monovalent cation channel TRPM4 regulates cell volume and has been implicated in cancer progression. TRPM4 was recently identified as a determinant of sensitivity to Acetalax (oxyphenisatin acetate) in triple-negative breast cancer and prostate cancer; however, whether TRPM4 also determines sensitivity to ErSO in prostate cancer cells had not been tested. Here, we investigate the relationship between ErSO, which induces TRPM4-associated cytotoxicity and ERα-positive breast cancer cell death, and TRPM4 expression in prostate cancer models. The Cancer Genome Atlas (TCGA) shows a broad range of TRPM4 expression in prostate cancers, and an integrated analysis of drug-response datasets reveals a positive association between TRPM4 expression and ErSO sensitivity in prostate cancer. Functional studies demonstrate that ErSO induces rapid cellular swelling, nuclear enlargement, and membrane blebbing selectively in TRPM4-high prostate cancer cells, consistent with early oncosis-like morphological responses, whereas TRPM4-low cells are less sensitive. Time-course analyses show a downregulation of TRPM4 following ErSO treatment. Chronic ErSO exposure results in the acquisition of resistance accompanied by loss of TRPM4 expression, and ErSO-resistant cells fail to undergo ErSO-induced morphological changes. Flow cytometry analyses further show that ErSO induces loss of membrane integrity and oncosis-like cell death-associated features in TRPM4-expressing cells. These findings establish TRPM4 as a functional determinant of ErSO responsiveness in prostate cancer cells and support its potential utility as a biomarker of ErSO sensitivity.

Significance Statement

We establish TRPM4 as a functional determinant and potential biomarker of ErSO responsiveness in prostate cancer cells. These findings identify TRPM4 expression as a potential marker for stratifying prostate cancer cells according to ErSO sensitivity.

Downloaded from aacrjournals.org/cancerrescommun/article-pdf/doi/10.1158/2767-9764.CRC-26-0215/3840575/crc-26-0215.pdf by National Institutes of Health user on 31 October 2026

Introduction

Prostate cancer is the second leading cause of cancer-related deaths among men worldwide (1). Novel therapeutic strategies and biomarkers that can predict treatment response remain needed.

Transient Receptor Potential Melastatin-4 (TRPM4) is a calcium-activated monovalent cation channel regulating membrane potential and intracellular calcium dynamics, thereby contributing to cell volume homeostasis (2-4). TRPM4 has been reported to be overexpressed in several human malignancies, including prostate cancer, where increased TRPM4 expression is observed in tumor tissues compared with benign prostate glands and is associated with clinical parameters such as biochemical recurrence (5-10). In prostate cancer models, TRPM4 upregulation has been associated with enhanced cell proliferation, migration, invasion and epithelial-to-mesenchymal transition, while TRPM4 loss reduces cellular outgrowth and metastatic potential (11,12). TRPM4-mediated alterations in calcium homeostasis and membrane depolarization are thought to influence these cancer-associated phenotypes, although the detailed mechanisms and drugs targeting TRPM4 (4,13-22) are under investigations.

ErSO (estrogen receptor–Selective Estrogen Degrader, or ERα activator–inhibitor) is a small molecule currently developed as an anticancer agent targeting estrogen receptor alpha (ERα)–positive tumors. Structurally related analogs, including ErSO-TFPy, have been developed and reported to induce rapid lytic stress responses in ERα-positive models in association with TRPM4 activation. These observations suggest that members of this compound class may engage overlapping but potentially distinct molecular mechanisms. Boudreau et al. (23) reported that ErSO induces rapid and selective destruction of ERα-positive breast cancer cells through hyperactivation of the unfolded protein response (UPR^ERα) pathway and markedly suppresses tumor growth in preclinical models. More recently, Ghosh et al. (21) demonstrated that ErSO activity correlates with TRPM4 expression across cancer models, suggesting a potential link between ErSO-induced cellular stress and TRPM4-dependent cell death. In these studies, ErSO was shown to induce rapid ATP depletion, cell swelling, and membrane disruption through hyperactivation of the unfolded protein response, leading to cell death with necrotic features. These studies primarily characterized ErSO-induced cytotoxicity based on metabolic collapse and loss of membrane integrity. However, whether similar temporal dynamics of early morphological stress responses and subsequent execution of cell death programs occur in non–ERα-driven malignancies, including prostate cancer, remains unknown. It is also unknown whether TRPM4 functions merely as a correlative marker of sensitivity or plays a mechanistic role in mediating cytotoxic responses in prostate cancer, and whether modulation of TRPM4 protein abundance contributes to therapeutic response or resistance.

Recent studies have expanded the therapeutic scope of ErSO and related lytic stress–inducing molecules. A single dose of ErSO has been reported to induce complete regression of large ERα-positive breast tumors in murine models, underscoring the potency of this rapid cell-destructive program in vivo (24). Moreover, necrosis-inducing analogs have demonstrated efficacy in ovarian cancer xenografts and patient-derived ascites organoids, with features consistent with immunogenic cell death responses (25).

Downloaded from aacrjournals.org/cancerrescommun/article-pdf/doi/10.1158/2767-9764.CRC-26-0215/3840575/crc-26-0215.pdf by National Institutes of Health user on 31 October 2026

These findings highlight the robust lytic capacity of this class of compounds. However, whether comparable TRPM4-associated mechanisms contribute to ErSO responsiveness in non–ERα-driven tumors, including prostate cancer, has not been explored.

We recently reported that the activity profiles of ErSO and Acetalax—a compound identified as inducing TRPM4-dependent cytotoxicity—are highly correlated across the NCI-60 cell line panel (20). We published that Acetalax and ErSO can be effective in hormone-independent Triple-Negative breast cancer (TNBC) cell lines (20), and that Acetalax is also effective in prostate cancer models in a TRPM4-dependent manner (26). These observations raise the possibility that TRPM4 may represent a shared determinant of sensitivity to ErSO in prostate cancer.

Here, we studied the relationship between ErSO-induced cytotoxicity and TRPM4 expression in three prostate cancer models with different TRPM4 expression levels and upon chronic exposure to ErSO. We sought to determine whether TRPM4 functionally contributes to ErSO responsiveness and whether dynamic changes in TRPM4 protein abundance are associated with therapeutic sensitivity or resistance. We demonstrate that ErSO induces rapid TRPM4-associated cellular swelling and oncosis-like morphological changes, followed by a delayed reduction in TRPM4 protein levels selectively in TRPM4-high prostate cancer cells, whereas TRPM4-low cells are resistant. Together, these findings support TRPM4 as a functional determinant and biomarker of ErSO sensitivity in prostate cancer and provide mechanistic insight into TRPM4-associated cell death responses induced by ErSO.

Materials and Methods

Patient transcript levels

Cancer types relevant to this study—prostate adenocarcinoma (PRAD), breast invasive carcinoma (BRCA), and ovarian serous cystadenocarcinoma (OV)—were selected for visualization. Box plots display the distribution of TRPM4 expression across individual patient samples, with statistical significance between tumor and normal groups calculated by GEPIA2 using a Student's t-test.

Normal versus tumor expression of TRPM4 was analyzed using the GEPIA2 (Gene Expression Profiling Interactive Analysis 2) platform, an interactive web-based resource for gene expression analysis of The Cancer Genome Atlas (TCGA) and The Genotype-Tissue Expression (GTEx) data (http://gepia2.cancer-pku.cn/).

TRPM4 expression was assessed using the Expression DIY module of GEPIA2, which enables customized comparison of gene expression between tumor and normal samples. Analyses were performed using RNA-seq expression data derived from TCGA tumors and matched normal tissues, with expression values represented as $\log_2(\text{TPM} + 1)$.

Cell lines and Reagents

The human prostate cancer cell lines PC3 (RRID: CVCL_0035) and LNCaP (RRID: CVCL_0395) were obtained from Dr. William D. Figg (National Institutes of

Downloaded from aacrjournals.org/cancerrescommun/article-pdf/doi/10.1158/2767-9764.CRC-26-0215/3840575/crc-26-0215.pdf by National Institutes of Health user on 31 October 2026

Health/National Cancer Institute, NIH/NCI) in October 2024 and authenticated by short tandem repeat (STR) profiling (Laragen). The DU145 cell line (RRID: CVCL_0105), originally obtained from the Developmental Therapeutics Program (DTP), was retrieved from frozen stocks maintained in our laboratory. DTP performs internal cell line authentication; however, the specific authentication method used for this cell line was not available to the authors, and additional authentication was not performed in our laboratory.

PC3 cells were maintained in F-12 medium (Thermo Fisher Scientific) supplemented with 10% fetal bovine serum (FBS; GeminiBio) and 1% penicillin–streptomycin (Gibco). LNCaP cells were cultured in RPMI 1640 medium (Thermo Fisher Scientific) supplemented with 10% FBS (GeminiBio) and 1% penicillin–streptomycin (Gibco). DU145 cells were maintained in DMEM (Thermo Fisher Scientific) containing 10% FBS (GeminiBio) and 1% penicillin–streptomycin (Gibco).

All cell lines were cultured at 37°C in a humidified incubator with 5% CO_2 and were routinely tested for mycoplasma contamination using the MycoAlert Mycoplasma Detection Kit (Lonza). The most recent testing was performed in March 2026, and all cell lines tested negative. Cells were used for experiments within 2 weeks after thawing. ErSO (NSC 835589) was obtained from the NCI Developmental Therapeutics Program (DTP).

Cell viability assay

Cells were seeded into 384-well plates at a density of 300 cells per well in 30 µL of culture medium and allowed to adhere for 24 hours. Cells were subsequently treated with ErSO at the indicated concentrations, as specified in the corresponding figures and figure legends. After 72 hours, cell viability was assessed using the ATPlite 1-Step Luminescence Assay System (PerkinElmer, Waltham, MA, USA) according to the manufacturer's instructions.

Luminescence was measured using a SpectraMax i3x microplate reader (Molecular Devices). Dose–response curves were generated and data were analyzed using GraphPad Prism version 10 (GraphPad Software Inc.). All experiments were performed in triplicate (n = 3).

TRPM4 knockdown and cell viability assay

TRPM4 knockdown (KD) was achieved in human prostate cancer PC3 cells using ON-TARGETplus SMARTpool siRNA targeting human TRPM4 (Horizon Discovery). To validate knockdown efficiency, PC3 cells were seeded at 2.0×10^5 cells per well in 6-well plates and transfected the following day with TRPM4 siRNA (final concentrations of 10 or 20 nM) or non-targeting control (NTC) siRNA using Lipofectamine RNAiMAX (Thermo Fisher Scientific) according to the manufacturer's instructions. TRPM4 protein expression was evaluated by Western blotting 72 h after transfection.

For drug sensitivity assays, reverse transfection was performed in 96-well plates by adding siRNA–Lipofectamine RNAiMAX complexes before cell seeding to achieve final siRNA concentrations of 10 or 20 nM. PC3 cells were seeded at 1,000 cells per well in 100 µL of complete growth medium and incubated for 72 h to allow TRPM4 depletion.

Downloaded from aacrjournals.org/cancerrescommun/article-pdf/doi/10.1158/2767-9764.CRC-26-0215/3840575/crc-26-0215.pdf by National Institutes of Health user on 31 October 2026

Cells were then treated with ErSO at the indicated concentrations by adding an equal volume of drug-containing medium and incubated for an additional 72 h. Cell viability was determined using the ATPlite assay as described above. Dose–response curves were generated using GraphPad Prism 10. All experiments were performed in technical triplicate.

Immunofluorescence staining and microscopy

Cells were seeded onto 24 × 60 mm glass coverslips placed in 8-well plates at a density of 1 × 10^5 cells per well in 500 µL of complete medium and allowed to adhere for 24 hours. Cells were then treated with ErSO as indicated in the figure legends. Following treatment, cells were washed with phosphate-buffered saline (PBS), fixed with 4% paraformaldehyde (PFA), permeabilized with 0.5% Triton X-100 in PBS, and blocked with 3% bovine serum albumin (BSA) in PBS-T for 1 hour at room temperature. After washing with PBS, cells were incubated with Alexa Fluor 488–conjugated phalloidin (A12379, Invitrogen) at a 1:200 dilution in PBS-T for 1 hour at room temperature. Cells were subsequently stained with DAPI (62248, Thermo Fisher Scientific) at a 1:1000 dilution for 30 minutes. Coverslips were mounted onto glass slides using ProLong Glass Antifade Mountant (P36980, Invitrogen). Fluorescence images were acquired using a Zeiss Axio Observer microscope (Carl Zeiss Microscopy GmbH) equipped with an Apotome 3 structured illumination module and a Plan-Apochromat 63×/1.4 NA oil-immersion objective.

Quantification of cell and nuclear size and membrane blebbing

Quantitative analyses of cell size, nuclear size, and membrane blebbing frequency were performed using fluorescence images acquired under identical imaging conditions with a Zeiss Axio Observer microscope. Images were collected from arbitrarily selected fields using a 63× objective, with each field containing approximately 2–40 cells. Cell and nuclear areas were measured using ImageJ2 software (version 2.14). For accurate quantification, adherent cells in close proximity were manually separated using ImageJ2 prior to measurement, and cells extending beyond the field of view were excluded from the analysis. Membrane blebbing was assessed by manual counting of cells exhibiting clear bleb formation. Quantitative results for cell swelling, nuclear enlargement, and blebbing frequency were visualized and plotted using GraphPad Prism version 10.

Immunoblotting

Cell pellets were collected, resuspended in PBS, and lysed by the addition of an equal volume of SDS sample buffer supplemented with 5% β-mercaptoethanol. Lysates were sonicated and heated at 95°C for 5 minutes. Protein concentrations were determined using the Bio-Rad Protein Assay Dye Reagent (Bio-Rad). Equal amounts of protein were resolved by reducing SDS–PAGE using precast gels (Invitrogen) and transferred onto polyvinylidene difluoride (PVDF) membranes (Millipore). Membranes were blocked and probed with the following primary antibodies: anti-TRPM4 [OTI10H5] (ab123936, Abcam, RRID: AB_10976061; 1:1000 dilution) and anti-GAPDH [6C5] (sc-32233, Santa Cruz Biotechnology; 1:2000 dilution). Primary antibody incubation was

Downloaded from aacrjournals.org/cancerrescommun/article-pdf/doi/10.1158/2767-9764.CRC-26-0215/3840575/crc-26-0215.pdf by National Institutes of Health user on 31 October 2026

performed overnight at 4 °C, followed by incubation with species-appropriate horseradish peroxidase (HRP)–conjugated secondary antibodies.

Protein bands were visualized using a ChemiDoc MP Imaging System (Bio-Rad) with SuperSignal™ West Pico PLUS or SuperSignal™ Ultimate Sensitivity Chemiluminescent Substrate (Thermo Fisher Scientific; 34580 or A38555).

Densitometric analyses were performed using Fiji/ImageJ with the Band/Peak Quantification Tool v1 macro as previously described (27). Briefly, images were converted to 8-bit grayscale and processed identically across all samples. Equal-sized rectangular regions of interest (ROIs) were applied to each lane, and background subtraction was performed using the same macro-defined parameters for all measurements. Integrated band intensities were obtained automatically and normalized to the corresponding GAPDH signal for each sample. GAPDH-normalized values were then expressed relative to the untreated control (control = 1) by dividing each value by the mean of the control group in Microsoft Excel. Normalized data were plotted using GraphPad Prism (GraphPad Software). Quantification was performed using independent biological samples (n=2). Data are presented as mean values with error bars indicating the range.

Generation of ErSO−resistant cells

ErSO-resistant prostate cancer cell lines were generated through chronic drug exposure. PC3 and LNCaP cells, which were initially sensitive to ErSO, were seeded at a density of 3×10^5 cells per 10-cm dish and maintained under continuous ErSO treatment. Cells were passaged upon reaching near confluency, typically every 1–2 weeks, with gradual escalation of ErSO concentration.

For ErSO selection, the initial concentration was set at 0.1 nM and increased in two-fold increments up to 12.8 nM. Thereafter, the concentration was increased in 10 nM increments starting from 20 nM. From 100 nM, the concentration was escalated in 20 nM increments, at which point PC3 cell proliferation was inhibited at 140 nM. For concentrations above 200 nM, ErSO levels were increased in 100 nM increments, and from 500 nM onward, concentrations were doubled at each step.

Under these conditions, PC3 cells chronically exposed to 120 nM ErSO were established as ErSO chronically exposed (ErSO-CE) cells. In contrast, LNCaP cells continued to proliferate even at the highest tested concentration of 10,000 nM (10 μM) ErSO and were therefore considered resistant. LNCaP cells maintained at 10 μM ErSO were established as a stable ErSO-resistant line.

Prior to all subsequent experiments, ErSO-CE cells were cultured in drug-free medium for at least two weeks to minimize acute drug effects.

Immunohistochemistry (cell line-derived samples)

Formalin-fixed, paraffin-embedded (FFPE) sections prepared from PC3 and DU145 cell pellets, either untreated (control) or treated with 0.1 μmol/L ErSO for 4 hours were used for TRPM4 immunohistochemistry (IHC). Antigen retrieval was performed by microwave heating in Antigen Retrieval Buffer (pH 6.0) (#ab93678, Abcam) for 20 minutes.

Downloaded from aacrjournals.org/cancerrescommun/article-pdf/doi/10.1158/2767-9764.CRC-26-0215/3840575/crc-26-0215.pdf by National Institutes of Health user on 31 October 2026

Sections were incubated with a mouse monoclonal anti-TRPM4 antibody (Abcam, #ab123936) at a 1:200 dilution in TBST (1× TBS containing 0.5% Tween 20) overnight at 4 °C. Following primary antibody incubation, sections were incubated for 30 minutes with N-Histofine Simple Stain MAX PO (MULTI) (Nichirei Biosciences Inc., #NIC-414151F). Signal detection was performed using DAB-3S chromogen (used at the manufacturer's recommended dilution; Nichirei Biosciences Inc., #415192F) with a 5-minute incubation at room temperature. DU145 cell pellets were included as a negative biological control because of their minimal TRPM4 expression. Stained sections were evaluated independently, and consensus regarding staining interpretation was reached in cases of discordant assessment.

Annexin V–FITC / Propidium Iodide (PI) Flow Cytometry Analyses

Apoptosis and cell death were analyzed by Annexin V–FITC and propidium iodide (PI) staining using the Annexin V–FITC Apoptosis Staining Detection Kit (ab14085, Abcam), according to the manufacturer's instructions. Cells were seeded in 6-well plates at a density of 1×10^5 cells per well and allowed to attach overnight. Cells were then treated with ErSO at the indicated concentrations for 2, 4, 6, 8, 15 or 24 hours. Following treatment, cells were harvested by trypsinization, washed with cold phosphate-buffered saline (PBS), and resuspended in Annexin V binding buffer. Cells were stained with Annexin V–FITC and propidium iodide (PI) as provided in the kit. In addition, PI staining was performed at a final concentration of 20 µg/mL (P3566, Thermo Fisher Scientific) and incubated for 15 minutes at 37 ℃ in the dark. Flow cytometric analysis was performed using a BD FACSCanto flow cytometer (Becton Dickinson). A minimum of 1×10^4 events were acquired per sample. Data were displayed with FITC fluorescence on the x-axis and PI fluorescence on the y-axis and were analyzed using FlowJo software version 10.10.0 (Becton Dickinson). Cell populations were classified as viable (Annexin V^-/PI^-), early apoptotic (Annexin V^+/PI^-), late apoptotic or secondary necrotic (Annexin V^+/PI^+), or necrotic/oncosis-like (Annexin V^-/PI^+).

Scatter plots

ESR1 and ESR2 expression data for breast, ovarian and prostate cancer cell lines were obtained from the Cancer Cell Line Encyclopedia (CCLE) via CellMinerCDB (https://discover.nci.nih.gov/cellminercdb/, RRID:SCR_025640). Scatter plots were generated using the "Univariate Analysis → Plot Data" function with tissue selection restricted to breast, ovary, and prostate cancer cell lines. Pearson correlation coefficients and corresponding p-values were calculated within CellMinerCDB (28). For Supplementary Figure S3, AR mRNA expression and ErSO activity were obtained from the NCI-60 dataset in CellMinerCDB (https://discover.nci.nih.gov/cellminercdb/, RRID:SCR_025640). Scatter plots were generated using the same function without restricting tissue type, and Pearson correlation coefficients and corresponding P values were calculated within CellMinerCDB. Prostate cancer cell lines were highlighted in the scatter plots.

Data Availability

Downloaded from aacrjournals.org/cancerrescommun/article-pdf/doi/10.1158/2767-9764.CRC-26-0215/3840575/crc-26-0215.pdf by National Institutes of Health user on 31 October 2026

The data generated in this study are available within the article and its supplementary data files. Publicly available data analyzed in this study were obtained from GEPIA2 (http://gepia2.cancer-pku.cn/) and CellMinerCDB (https://discover.nci.nih.gov/cellminercdb/). Additional data are available from the corresponding authors upon reasonable request.

Results

TRPM4 expression is associated with ErSO sensitivity in prostate cancer

To explore the potential association between TRPM4 expression and sensitivity to ErSO, we first examined TRPM4 expression in cancer patient datasets. Analysis of The Cancer Genome Atlas (TCGA) showed that TRPM4 is expressed across multiple tumor types relevant to ErSO biology, including prostate, breast, and ovarian cancers with prostate cancer being the highest (6,8). Notably, prostate adenocarcinoma (PRAD) exhibited significantly higher TRPM4 expression in tumor tissues compared with corresponding normal prostate samples (Figure 1A).

We next assessed basal TRPM4 protein expression in three commonly used prostate cancer cell lines. Immunoblot analysis demonstrated that PC3 and LNCaP cells express relatively high levels of TRPM4 protein, whereas DU145 cells exhibit low TRPM4 expression (Figure 1B), establishing a panel of prostate cancer models with differential TRPM4 status.

Dose–response analyses showed that TRPM4-high prostate cancer cell lines (PC3 and LNCaP) are markedly more sensitive to ErSO treatment than the TRPM4-low DU145 cells (Figure 1C). Although both PC3 and LNCaP cells express TRPM4, the magnitude of ErSO sensitivity differed between these models, suggesting that additional cellular factors may modulate response among TRPM4-positive cells.

Together, these data demonstrate that TRPM4 expression is associated with ErSO sensitivity in prostate cancer models and provided a rationale for subsequent functional studies investigating the role of TRPM4 in mediating ErSO-induced cellular responses.

TRPM4 knockdown reduces ErSO sensitivity in PC3 cells

To functionally assess the role of TRPM4 in ErSO responsiveness, we performed siRNA-mediated knockdown of TRPM4 in PC3 cells. Immunoblotting confirmed efficient reduction of TRPM4 protein expression following treatment with TRPM4 siRNA at 10 nM and 20 nM (Figure 2A).

Dose–response analyses showed that TRPM4 knockdown reduced ErSO sensitivity, as indicated by a rightward shift of the dose–response curves compared with non-targeting control cells (Figure 2B). These results provide functional evidence that TRPM4 contributes to ErSO responsiveness in prostate cancer cells.

ErSO rapidly induces cell swelling and membrane blebbing in TRPM4-high prostate cancer cells

Given the association between TRPM4 expression and ErSO sensitivity, we next investigated early cellular responses to ErSO. TRPM4-high PC3 cells were exposed to

Downloaded from aacrjournals.org/cancerrescommun/article-pdf/doi/10.1158/2767-9764.CRC-26-0215/3840575/crc-26-0215.pdf by National Institutes of Health user on 31 October 2026

ErSO (0.1 μM) and monitored by fluorescence microscopy over a short time course. Within minutes of treatment, PC3 cells exhibited marked cellular enlargement and membrane blebbing, which became progressively more pronounced from 5 to 60 minutes (Figure 3A).

Quantitative image analysis confirmed significant increases in cell area and nuclear area, as well as an increased fraction of cells displaying membrane blebbing following ErSO treatment in PC3 cells (Figure 3B). In contrast, under identical conditions, TRPM4-low DU145 cells showed no significant changes in cell size, nuclear size, or membrane morphology (Figure 3C, D).

Together, these data indicate that ErSO triggers rapid cell swelling, nuclear enlargement, and membrane remodeling preferentially in TRPM4-high prostate cancer cells, consistent with early oncosis-like morphological responses occurring shortly after ErSO exposure.

ErSO induces loss of membrane integrity and oncosis-like cell death–associated features in prostate cancer cells with high TRPM4 expression

To determine whether the rapid morphological changes induced by ErSO progress to cell death, we performed Annexin V/propidium iodide (PI) flow cytometric analyses. In TRPM4-high PC3 cells, ErSO caused a time-dependent redistribution of cell populations from the viable fraction (Annexin V^-/PI^-) toward Annexin V– and PI-positive populations. A marked increase in PI-positive cells was observed between 4 and 8 hours after treatment, indicating early loss of plasma membrane integrity (Figure 4A and B). Prolonged ErSO exposure further accentuated this effect. After 15 and 24 hours of treatment, PC3 cells exhibited substantial accumulation of Annexin V^+/PI^+ cells, consistent with late-stage cell death accompanied by sustained membrane disruption.

In contrast, TRPM4-low DU145 cells showed minimal changes in Annexin V or PI staining and largely remained unaffected by ErSO under identical treatment conditions (Figure 4C).

Together, these data demonstrate that ErSO induces a TRPM4-dependent loss of membrane integrity and cell death–associated responses consistent with necrotic/oncosis-like features in prostate cancer cells. The absence of this response in cells lacking TRPM4 expression supports a functional contribution of TRPM4 in mediating ErSO-induced cytotoxicity.

ErSO downregulates TRPM4 protein in ErSO-sensitive prostate cancer cells

Because we recently observed that Acetalax or bisaccodyl, which are chemically related to ErSO, induce TRPM4 degradation (22), we examined whether ErSO also affects TRPM4 protein levels. Time-course analyses in PC3 cells showed that ErSO induces the loss of TRPM4 protein beginning within 2 hours after exposure and becoming more pronounced at later time points (Figure 5A). Quantitative densitometric analysis confirmed the time-dependent decrease in TRPM4 protein levels following ErSO treatment.

Downloaded from aacrjournals.org/cancerrescommun/article-pdf/doi/10.1158/2767-9764.CRC-26-0215/3840575/crc-26-0215.pdf by National Institutes of Health user on 31 October 2026

This reduction in TRPM4 protein was detected beginning approximately 2 hours after ErSO exposure, whereas early morphological changes including cell swelling and membrane blebbing, occurred within 5 to 60 minutes (see Figures 3 & 4). This temporal sequence indicates that TRPM4 downregulation follows, rather than precedes, the initial morphological responses induced by ErSO.

Consistent with the immunoblotting results, immunohistochemical analysis of cultured PC3 cell pellets demonstrated reduced TRPM4 staining intensity accompanied by disrupted cellular morphology after 4 hours of ErSO treatment, compared with untreated controls (Figure 5B, C). In contrast, DU145 cells, which express low basal levels of TRPM4 and are resistant to ErSO, showed no detectable TRPM4 immunoreactivity in the absence and presence of ErSO (Figure 5B, C).

Collectively, these data indicate that TRPM4 can readily be detected by immunohistochemistry at the surface of tumor cells and that ErSO induces a reduction of TRPM4 protein selectively in ErSO-sensitive prostate cancer cells, occurring after the onset of early morphological and subsequent membrane changes.

Chronic ErSO exposure leads to loss of TRPM4 expression and acquisition of ErSO resistance

To further examine the functional relationship between TRPM4 expression and ErSO sensitivity, we generated ErSO-resistant prostate cancer cell lines through chronic drug exposure. Parental PC3 and LNCaP cells were subjected to stepwise increases in ErSO concentration over multiple passages until stable chronically exposed derivatives (ErSO-CE) were established (Figure 6A).

Dose–response analyses revealed a pronounced rightward shift in IC50 values in PC3-CE cells compared with parental PC3 cells, indicating a substantial reduction in ErSO sensitivity following chronic exposure (Figure 6B). Immunoblot analyses demonstrated that this acquired resistance was accompanied by a marked reduction or loss of TRPM4 protein expression in PC3-CE cells (Figure 6C). Similar results were obtained in LNCaP-derived ErSO-CE cells, which retained proliferative capacity despite prolonged ErSO exposure and exhibited reduced TRPM4 expression (Figure 6B, C).

In the resistant cells with TRPM4 loss, acute ErSO treatment failed to induce cellular swelling, nuclear enlargement, or membrane blebbing in PC3-CE cells, in contrast to the robust morphological responses observed in parental PC3 cells (Figure 6D, E).

Flow cytometry analyses also showed that ErSO-CE cells did not undergo Annexin V or propidium iodide positivity following ErSO treatment, indicating preservation of membrane integrity and absence of ErSO-induced cell death (Supplementary Figure S1). This resistance phenotype closely paralleled that observed in TRPM4-low DU145 cells.

Collectively, these findings demonstrate that chronic ErSO exposure selects for prostate cancer cells with diminished TRPM4 expression and loss of ErSO-induced morphological changes, membrane destabilization and cell death.

Discussion

Downloaded from aacrjournals.org/cancerrescommun/article-pdf/doi/10.1158/2767-9764.CRC-26-0215/3840575/crc-26-0215.pdf by National Institutes of Health user on 31 October 2026

In this study, we identify TRPM4 as a determinant and potential biomarker of ErSO sensitivity in prostate cancer cells and provide mechanistic insights into the temporal sequence of cellular events underlying ErSO-induced cytotoxicity. By integrating public datasets with functional analyses in prostate cancer models, we demonstrate that ErSO preferentially targets TRPM4-high cells, inducing rapid cell swelling and membrane remodeling followed by TRPM4 protein loss and cell death characterized by loss of membrane integrity and cell swelling. Importantly, chronic ErSO exposure selects for TRPM4-deficient cells that are functionally resistant to ErSO, supporting the association between TRPM4 expression and ErSO responsiveness.

Previous studies have characterized ErSO as a potent anticancer agent primarily in ERα-positive breast cancer, where it induces catastrophic cell death, which had been associated with hyperactivation of the unfolded protein response (UPR^ERα) (21). More recently, correlative analyses suggested that TRPM4 expression tracks with ErSO and Acetalax activity across diverse cancer cell lines (20-22,26). However, whether TRPM4 directly contributes to ErSO-induced cytotoxicity in non–ERα-driven malignancies had not been explored. Our findings demonstrate that TRPM4 is a determinant of ErSO responsiveness in prostate cancer, a tumor type not defined by estrogen receptor signaling, thereby broadening the biological and therapeutic scope of ErSO activity.

Consistent with this distinction, the prostate cancer cell lines used in this study exhibit low *ESR1* and *ESR2* expression compared with most other cancer cell lines (Supplementary Figure S2), consistent with the ErSO responses observed here occurring in a low-ER-expression context. Furthermore, analysis of publicly available datasets did not reveal a significant association between AR mRNA expression and ErSO activity across the NCI-60 cell line panel (Supplementary Figure S3). However, these analyses do not directly address ErSO sensitivity in androgen-dependent or AR inhibitor-resistant prostate cancer models.

A notable feature of ErSO is the temporal dissociation between early cellular responses and subsequent TRPM4 downregulation. ErSO induces rapid cell swelling, nuclear enlargement and membrane blebbing within minutes in TRPM4-high cells, whereas detectable reduction of TRPM4 protein occurred several hours later.

Flow cytometry analyses suggest a dynamic shift in cell death populations over time. At early time points, ErSO increased Annexin V–positive cells, suggesting activation of apoptotic signaling in parallel with membrane swelling. At later time points, a progressive accumulation of PI-positive and Annexin V^+/PI^+ populations were observed, consistent with loss of membrane integrity and transition toward necrotic or oncosis-like cell death. This mode of cell death has been referred to as oncosis (22) but more recently as necrotic cell death by sodium overload (NECSO) (4).

These observations suggest that TRPM4-associated ionic dysregulation contributes to a rapid osmotic imbalance, culminating in massive cell swelling and membrane destabilization (21). TRPM4 is a calcium-activated monovalent cation channel regulating membrane potential and cell volume homeostasis (4,11,12,29). ErSO, Acetalax as well as their chemically related derivative Necrocide-1 (NC1) have been proposed to act as TRPM4 agonists trapping the TRPM4 sodium channel in an open configuration (4,20,21). This has been characterized most extensively in ERα-positive

Downloaded from aacrjournals.org/cancerrescommun/article-pdf/doi/10.1158/2767-9764.CRC-26-0215/3840575/crc-26-0215.pdf by National Institutes of Health user on 31 October 2026

and ERα-negative breast cancer cells (20,21). In this context, our findings in ERα-negative prostate cancer cells extend the ErSO response framework to a distinct lineage and support the idea that TRPM4 status can stratify susceptibility to ErSO-induced membrane stress and late-stage cell death. Consistent with this temporal model and our previous studies with Acetalax and Bisacodyl (20,26), immunoblotting and immunohistochemical analyses demonstrated a delayed downregulation of TRPM4 protein in ErSO-sensitive PC3 cells (Figure 5).

The selective targeting of TRPM4 by ErSO is supported by our chronic exposure experiments. Long-term ErSO treatment selected for prostate cancer cells with reduced TRPM4 expression, loss of ErSO induced morphological changes and resistance to cell death. This adaptive phenotype mirrors the intrinsic resistance observed in TRPM4-low DU145 cells and supports a functional relationship between TRPM4 expression and ErSO sensitivity. Nevertheless, the partial sensitivity of TRPM4-low DU145 cells to ErSO suggests that additional cellular factors beyond TRPM4 are also likely to contribute to the overall response. While the mechanisms driving TRPM4 loss under chronic ErSO exposure remain to be elucidated, these findings suggest that TRPM4 status may influence therapeutic durability and resistance evolution.

From a translational perspective, our findings nominate TRPM4 as a potential predictive companion diagnostic (CDx) biomarker for ErSO response. TRPM4 expression varies widely across tumor types and even among prostate cancer subtypes (5,8), suggesting that patient selection based on TRPM4 status could improve treatment precision and therapeutic efficacy. Moreover, the convergence of cellular responses to ErSO, Acetalax and NC1 (4,21,26) with TRPM4 expression raises the possibility that vulnerabilities related to TRPM4-dependent regulation of cell volume and membrane integrity warrant further investigation across cancer models (4,13-20,26).

Several limitations should be acknowledged. Our study was conducted primarily in cell line–based models, and additional follow-up studies are warranted to establish the relevance of TRPM4-dependent ErSO responses *in vivo*. While our data support a functional role for TRPM4 in mediating ErSO-induced cytotoxicity, whether ErSO directly or indirectly activates the TRPM4 channels will require structural and biochemical investigations. Elucidating the upstream signaling events linking ErSO exposure to TRPM4-dependent membrane stress will also be an important direction for future studies. Although the present study focuses on TRPM4-associated morphological changes, membrane integrity and Annexin V/PI flow cytometry to characterize ErSO-induced cell death, further characterization of downstream cell death regulatory pathways, including apoptotic and survival signaling proteins, would provide additional mechanistic insight and represents an important direction for future studies. The present study did not directly evaluate ErSO sensitivity in androgen-dependent or AR inhibitor-resistant prostate cancer models and therefore does not establish a relationship between ErSO responsiveness and castration resistance. Future studies using established AR inhibitor-resistant models will be required to address this question. Additional studies using genetic knockout systems and a broader panel of prostate cancer models will be required to further define the relative contributions of TRPM4-dependent and TRPM4-independent mechanisms to ErSO responsiveness.

Downloaded from aacrjournals.org/cancerrescommun/article-pdf/doi/10.1158/2767-9764.CRC-26-0215/3840575/crc-26-0215.pdf by National Institutes of Health user on 31 October 2026

Authors' Disclosures

NT: Consultant/ Advisor for ATX, CorriXR Therapeutics, and FRONTEO.
YP: Consultant for Sutro, PharmaMar and Amgen. Co-Chair of the Research Council of the Bloom Syndrome Association (BSA).

Authors' Contributions

Design: Y.H-K, W.C.R, N.T, Y.P.
Experiments: Y.H-K, D.T.
Manuscript: Y.H-K, W.C.R, N.T, Y.P
Supervisor: Y.P, W.C.R, N.T

Acknowledgments

We would like to thank Dr. William D. Figg, National Institutes of Health/National Cancer Institute (NIH/NCI) for the kind gift of the LNCaP and PC3 cell lines. We would like to thank Makito Mizunuma and Yoshihito Yokoyama, Hirosaki University for helpful discussions and advice.

This research was supported by the Intramural Research Program of the National Institutes of Health (NIH), Center for Cancer Research, National Cancer Institute (Z01 BC 006150). Additional support was provided by the Stephenson Cancer Center through internal resources and P30 CA225520.

Generative artificial intelligence (ChatGPT, OpenAI) was used to improve the quality and clarity of the English writing in specific sections of the manuscript. All AI-assisted revisions were reviewed and approved by the authors, who take full responsibility for the accuracy and integrity of the final manuscript.

Disclaimer

The contributions of the NIH author(s) were made as part of their official duties as NIH federal employees, are in compliance with agency policy requirements, and are considered Works of the United States Government. However, the findings and conclusions presented in this paper are those of the author(s) and do not necessarily reflect the views of the NIH or the U.S. Department of Health and Human Services.

Downloaded from aacrjournals.org/cancerrescommun/article-pdf/doi/10.1158/2767-9764.CRC-26-0215/3840575/crc-26-0215.pdf by National Institutes of Health user on 31 October 2026

References

1. Sung H, Ferlay J, Siegel RL, Laversanne M, Soerjomataram I, Jemal A*, et al.* Global Cancer Statistics 2020: GLOBOCAN Estimates of Incidence and Mortality Worldwide for 36 Cancers in 185 Countries. CA Cancer J Clin **2021**;71(3):209-49 doi 10.3322/caac.21660.
2. Launay P, Fleig A, Perraud AL, Scharenberg AM, Penner R, Kinet JP. TRPM4 is a Ca2+-activated nonselective cation channel mediating cell membrane depolarization. Cell 2002;109(3):397-407 doi 10.1016/s0092-8674(2)00719-5.
3. Nilius B, Owsianik G, Voets T, Peters JA. Transient receptor potential cation channels in disease. Physiol Rev 2007;87(1):165-217 doi 10.1152/physrev.00021.2006.
4. Fu W, Wang J, Li T, Qiao Y, Zhang Z, Zhang X, et al. Persistent activation of TRPM4 triggers necrotic cell death characterized by sodium overload. Nat Chem Biol 2025;21(6):1238-49 doi 10.1038/s41589-025-01841-3.
5. Berg KD, Soldini D, Jung M, Dietrich D, Stephan C, Jung K, et al. TRPM4 protein expression in prostate cancer: a novel tissue biomarker associated with risk of biochemical recurrence following radical prostatectomy. Virchows Arch 2016;468(3):345-55 doi 10.1007/s00428-015-1880-y.
6. Ashida S, Nakagawa H, Katagiri T, Furihata M, Iiizumi M, Anazawa Y, et al. Molecular features of the transition from prostatic intraepithelial neoplasia (PIN) to prostate cancer: genome-wide gene-expression profiles of prostate cancers and PINs. Cancer Res 2004;64(15):5963-72 doi 10.1158/0008-5472.CAN-04-0020.
7. Holzmann C, Kappel S, Kilch T, Jochum MM, Urban SK, Jung V, et al. Transient receptor potential melastatin 4 channel contributes to migration of androgen-insensitive prostate cancer cells. Oncotarget 2015;6(37):41783-93 doi 10.18632/oncotarget.6157.
8. Kristiansen G, Pilarsky C, Wissmann C, Kaiser S, Bruemmendorf T, Roepcke S, et al. Expression profiling of microdissected matched prostate cancer samples reveals CD166/MEMD and CD24 as new prognostic markers for patient survival. J Pathol 2005;205(3):359-76 doi 10.1002/path.1676.
9. Sagredo AI, Sagredo EA, Cappelli C, Baez P, Andaur RE, Blanco C, et al. TRPM4 regulates Akt/GSK3-beta activity and enhances beta-catenin signaling and cell proliferation in prostate cancer cells. Mol Oncol 2018;12(2):151-65 doi 10.1002/1878-0261.12100.
10. Schinke EN, Bii V, Nalla A, Rae DT, Tedrick L, Meadows GG, et al. A novel approach to identify driver genes involved in androgen-independent prostate cancer. Mol Cancer 2014;13:120 doi 10.1186/1476-4598-13-120.
11. Bochen F, Subedi S, La Manna F, Jarrin S, Papapostolou I, Kruithof-de Julio M, et al. TRPM4 contributes to cell death in prostate cancer tumor spheroids, and to extravasation and metastasis in a zebrafish xenograft model system. Mol Oncol 2025;19(3):1299-309 doi 10.1002/1878-0261.13795.
12. Sagredo AI, Sagredo EA, Pola V, Echeverria C, Andaur R, Michea L, et al. TRPM4 channel is involved in regulating epithelial to mesenchymal transition, migration, and invasion of prostate cancer cell lines. J Cell Physiol 2019;234(3):2037-50 doi 10.1002/jcp.27371.

Downloaded from aacrjournals.org/cancerrescommun/article-pdf/doi/10.1158/2767-9764.CRC-26-0215/3840575/crc-26-0215.pdf by National Institutes of Health user on 31 October 2026

13. Arullampalam P, Preti B, Ross-Kaschitza D, Lochner M, Rougier JS, Abriel H. Species-Specific Effects of Cation Channel TRPM4 Small-Molecule Inhibitors. Front Pharmacol 2021;12:712354 doi 10.3389/fphar.2021.712354.
14. Delalande C, Awale M, Rubin M, Probst D, Ozhathil LC, Gertsch J, et al. Optimizing TRPM4 inhibitors in the MHFP6 chemical space. Eur J Med Chem 2019;166:167-77 doi 10.1016/j.ejmech.2019.01.048.
15. Niu L, Liu H, Li X, Wang L, Hua H, Cao Q, et al. Design, synthesis, and biological evaluation of 2-(naphthalen-1-yloxy)-N-phenylacetamide derivatives as TRPM4 inhibitors for the treatment of prostate cancer. Bioorg Med Chem 2024;98:117584 doi 10.1016/j.bmc.2023.117584.
16. Ozhathil LC, Rougier JS, Arullampalam P, Essers MC, Ross-Kaschitza D, Abriel H. Deletion of Trpm4 Alters the Function of the Na(v)1.5 Channel in Murine Cardiac Myocytes. Int J Mol Sci 2021;22(5) doi 10.3390/ijms22073401.
17. Preti B, Rougier JS, Papapostolou I, Bochen F, Gerber CE, Abriel H, et al. Targeting Ion Channel TRPM4. Chimia (Aarau) 2022;76(10):1039-44 doi 10.2533/chimia.2022.1039.
18. Stoklosa P, Borgstrom A, Hauert B, Baur R, Peinelt C. Investigation of Novel Small Molecular TRPM4 Inhibitors in Colorectal Cancer Cells. Cancers (Basel) 2021;13(19) doi 10.3390/cancers13215400.
19. Sun M, Wang L, Cao Q, Wang X, Zhang Y, Guo M, et al. Discovery of HZS60 as a Novel Brain Penetrant NMDAR/TRPM4 Interaction Interface Inhibitor with Improved Activity and Pharmacokinetic Properties for the Treatment of Cerebral Ischemia. J Med Chem 2025;68(2):2008-43 doi 10.1021/acs.jmedchem.4c02772.
20. Reinhold WC, Marangoni E, Elloumi F, Montagne R, Varma S, Wang Y, et al. Acetalax and Bisacodyl for the Treatment of Triple-Negative Breast Cancer: A Combined Molecular and Preclinical Study. Cancer Res Commun 2025;5(2):375-88 doi 10.1158/2767-9764.CRC-24-0435.
21. Ghosh S, Yang R, Duraki D, Zhu J, Kim JE, Jabeen M, et al. Plasma Membrane Channel TRPM4 Mediates Immunogenic Therapy-Induced Necrosis. Cancer Res 2023;83(16):3115-30 doi 10.1158/0008-5472.CAN-23-0157.
22. Mizunuma M, Redon CE, Saha LK, Tran AD, Dhall A, Sebastian R, et al. Acetalax (Oxyphenisatin Acetate, NSC 59687) and Bisacodyl Cause Oncosis in Triple-Negative Breast Cancer Cell Lines by Poisoning the Ion Exchange Membrane Protein TRPM4. Cancer Res Commun 2024;4(6):2101-11 doi 10.1158/2767-9764.CRC-24-0093.
23. Boudreau MW, Duraki D, Wang L, Mao C, Kim JE, Henn MA, et al. A small-molecule activator of the unfolded protein response eradicates human breast tumors in mice. Sci Transl Med 2021;13(601) doi 10.1126/scitranslmed.abf1383.
24. Duraki D, Jabeen M, Mao C, Wang L, Ghosh S, Dai X, et al. A necrosis inducer promotes an immunogenic response and destroys ovarian cancers in mouse xenografts and patient ascites organoids. Cancer Lett 2025;625:217738 doi 10.1016/j.canlet.2025.217738.
25. Mulligan MP, Boudreau MW, Bouwens BA, Lee Y, Carrell HW, Zhu J, et al. Single Dose of a Small Molecule Leads to Complete Regressions of Large Breast Tumors in Mice. ACS Cent Sci 2025;11(2):228-38 doi 10.1021/acscentsci.4c01628.

Downloaded from aacrjournals.org/cancerrescommun/article-pdf/doi/10.1158/2767-9764.CRC-26-0215/3840575/crc-26-0215.pdf by National Institutes of Health user on 31 October 2026

26. Hoshi-Kadonosawa Y, Reinhold WC, Taniyama D, Inoue Y, Luna A, Kumar S, et al. TRPM4 Expression as a Predictive Biomarker and a Mechanistic Driver of Acetalax Activity in Prostate Cancer: Preclinical Efficacy Studies. Mol Cancer Ther 2026 doi 10.1158/1535-7163.MCT-26-0011.
27. Ohgane K, Yoshioka H. Quantification of gel bands by an ImageJ macro, Band/Peak Quantification Tool v1. Protocolsio 2019 doi 10.17504/protocols.io.7vghn3w.
28. Luna A, Elloumi F, Varma S, Wang Y, Rajapakse VN, Aladjem MI, et al. CellMiner Cross-Database (CellMinerCDB) version 1.2: Exploration of patient-derived cancer cell line pharmacogenomics. Nucleic Acids Res 2021;49(D1):D1083-D93 doi 10.1093/nar/gkaa968.
29. Teixeira-Duarte CM, Zeng W, Jiang Y. Structural landscape of activation, desensitization and inhibition in the human TRPM4 channel. Nat Struct Mol Biol 2026;33(1):43-52 doi 10.1038/s41594-025-01705-3.

Downloaded from aacrjournals.org/cancerrescommun/article-pdf/doi/10.1158/2767-9764.CRC-26-0215/3840575/crc-26-0215.pdf by National Institutes of Health user on 31 October 2026

Figure legends

Figure 1. TRPM4 expression and its association with ErSO sensitivity.
(A) Boxplots of TRPM4 mRNA expression in tumor and normal tissues from selected TCGA cancer types relevant to ErSO biology and this study, including prostate adenocarcinoma (PRAD), breast invasive carcinoma (BRCA) and ovarian serous cystadenocarcinoma (OV). Expression levels are shown as log2(TPM+1). Tumor tissues are shown in red and normal tissues in gray.
(B) Representative Western blot visualizing basal TRPM4 protein expression in the prostate cancer cell lines LNCaP, PC3 and DU145. GAPDH was used as a loading control. PC3 and LNCaP cells exhibit high TRPM4 expression, whereas DU145 cells have no detectable TRPM4.
(C) Cell-viability assay dose–response curves of prostate cancer cell lines treated with ErSO for 72 hours. TRPM4-high cell lines (PC3 and LNCaP) exhibit greater sensitivity compared with the TRPM4-low cell line DU145. Data are shown as mean ± SEM.

Figure 2. TRPM4 knockdown reduces ErSO sensitivity.
(A) Representative immunoblot showing TRPM4 protein expression in PC3 cells transfected with non-targeting control (NTC) siRNA or TRPM4-targeting siRNA (10 or 20 nM) for 72 h. TRPM4 protein levels were normalized to GAPDH, and relative protein expression is shown below. Data are presented relative to the NTC control.
(B) Dose–response curves of PC3 cells transfected with NTC or TRPM4-targeting siRNA and treated with the indicated concentrations of ErSO for 72 h. TRPM4 knockdown resulted in reduced sensitivity to ErSO compared with NTC-transfected cells. Cell viability was measured using the ATPlite assay. Data are presented as mean ± SD from technical triplicates.

Figure 3. ErSO induces rapid TRPM4-dependent cellular swelling, nuclear enlargement, and membrane blebbing in prostate cancer cells.
(A) Confocal microscopy of time-dependent morphological changes in TRPM4-high PC3 cells following ErSO treatment. Representative images of PC3 cells treated with ErSO (0.1 μM) for 5, 30 or 60 minutes. Cells were stained with DAPI (nuclei, blue) and phalloidin (F-actin, green). Progressive increases in cell size and membrane blebbing were observed beginning between 5–30 minutes. Scale bars: 20 μm.
(B) Scatter plot quantitative analysis of swelling and blebbing in PC3 cells.
Violin plots and bar graphs show cell area, nuclear area and membrane blebbing at different drug exposure time points. Data were collected from ≥ 200 cells per condition in ≥ 3 biologically independent experiments. Statistical analysis was performed using the Kruskal-Wallis test followed by Dunn's multiple comparisons test (GraphPad Prism 10). ****P < 0.0001, **P < 0.01, *P < 0.05. ErSO induces a rapid and significant increase in swelling and blebbing, consistent with early oncosis-like membrane disruption.
(C) TRPM4-low DU145 cells do not undergo morphological changes upon ErSO treatment. Representative images of DU145 cells treated with ErSO for the same time points as panels A-B. Scale bars: 20 μm.
(D) Scatter plot quantitative analysis of DU145 morphology following ErSO exposure.

Downloaded from aacrjournals.org/cancerrescommun/article-pdf/doi/10.1158/2767-9764.CRC-26-0215/3840575/crc-26-0215.pdf by National Institutes of Health user on 31 October 2026

Violin plots and bar graphs demonstrate no statistically significant changes in cell size, nuclear area or blebbing in DU145 cells following ErSO treatment. Analysis was performed as in panel B.

Figure 4. ErSO induces time-dependent loss of membrane integrity in TRPM4-high prostate cancer cells.
(A) Flow cytometry of representative Annexin V–FITC/propidium iodide (PI) plots of TRPM4-high PC3 cells treated with ErSO (0.1 μM) for the indicated times (2, 4, 6, 8, and 24 hours). A progressive shift from viable cells ($FITC^-/PI^-$) toward PI-positive populations is observed over time.
(B) Bar graph summarizing the percentage of PC3 cells in each population ($FITC^-/PI^-$, $FITC^+/PI^-$, $FITC^+/PI^+$) at the indicated time points following ErSO treatment.
(C) Flow cytometry of representative Annexin V–FITC/PI flow cytometry plots and corresponding population percentages for TRPM4-low DU145 cells treated with ErSO (0.1 μM) for 24 hours. Minimal changes were observed compared with untreated controls, consistent with resistance to ErSO-induced cell death.

Figure 5. ErSO induces TRPM4 protein downregulation in ErSO-sensitive prostate cancer cells.
(A) Representative immunoblot showing time-dependent downregulation of TRPM4 protein levels in ErSO-sensitive PC3 cells treated with ErSO (0.1 μM). GAPDH was used as loading control. The bar graph shows densitometric quantification of TRPM4 protein levels normalized to GAPDH and relative to untreated controls.
(B) Immunohistochemical analysis of TRPM4 in cultured cell pellets treated with ErSO (0.1 μM) for 4 hours. Representative images show reduced TRPM4 immunoreactivity in ErSO-treated PC3 cells compared with untreated controls, whereas DU145 cells display minimal TRPM4 staining under both conditions.
(C) Hematoxylin and eosin (H&E) staining of cultured PC3 and DU145 cell pellets treated with ErSO (0.1 μM) for 4 hours. ErSO-treated PC3 cells exhibit altered cellular morphology compared with untreated controls, while DU145 cells show no overt morphological changes.

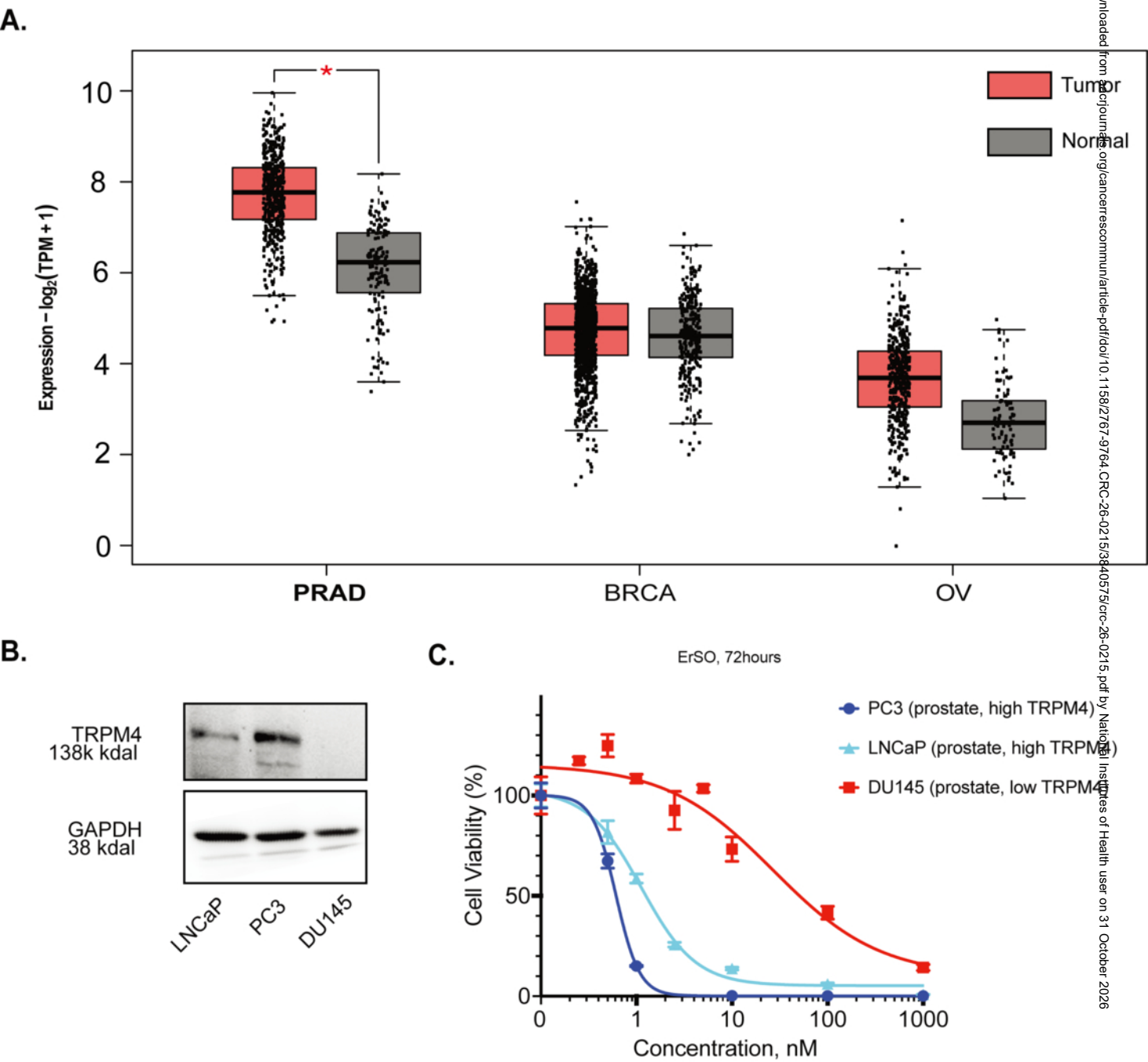
Figure 6. Chronic exposure to ErSO induces TRPM4 loss and acquisition of resistance in prostate cancer cells.
(A) Schematic of the chronic ErSO exposure protocol used to generate the ErSO-resistant cell lines. PC3 and LNCaP parental cells were exposed to stepwise increasing concentrations of ErSO over multiple passages until stable resistant derivatives (ErSO-CE) were obtained. Drug concentrations and treatment intervals used during the selection process are indicated.
(B) Cell viability assay in ErSO-CE cells following chronic drug adaptation. Dose–response curves demonstrating cell viability after 72 h ErSO treatment in parental versus ErSO-CE cell lines. PC3 parental cells are highly sensitive to ErSO, whereas PC3-CE cells show marked right-shifted dose–response curves and increased IC50 values. LNCaP cells demonstrated low sensitivity at baseline and further reduced responsiveness following chronic exposure. Data represent mean ± SEM from ≥ 3 biologically independent experiments.

Downloaded from aacrjournals.org/cancerrescommun/article-pdf/doi/10.1158/2767-9764.CRC-26-0215/3840575/crc-26-0215.pdf by National Institutes of Health user on 31 October 2026

(C) Loss of TRPM4 protein expression in ErSO-resistant cells. Representative immunoblot comparing TRPM4 expression in parental (WT) and ErSO-CE PC3 and LNCaP cells. GAPDH served as loading control.
(D) Confocal fluorescence imaging of morphological response to acute ErSO exposure in ErSO-CE cells. PC3 parental and PC3-CE cells treated with ErSO (0.1 μM, 30 min). Parental PC3 cells exhibited robust swelling and membrane blebbing whereas PC3-CE cells showed minimal morphological change. Scale bars: 20 μm.
(E) Quantitative analysis of ErSO response in parental versus ErSO-CE PC3 cells. Violin plots and bar graphs summarize cell swelling, nuclear enlargement and membrane blebbing. Data were collected from ≥ 200 cells per condition across ≥ 3 biological replicates. Statistical analysis was performed using the Kruskal–Wallis test with Dunn's multiple comparisons test (GraphPad Prism 10). ****P < 0.0001, **P < 0.01, *P < 0.05.

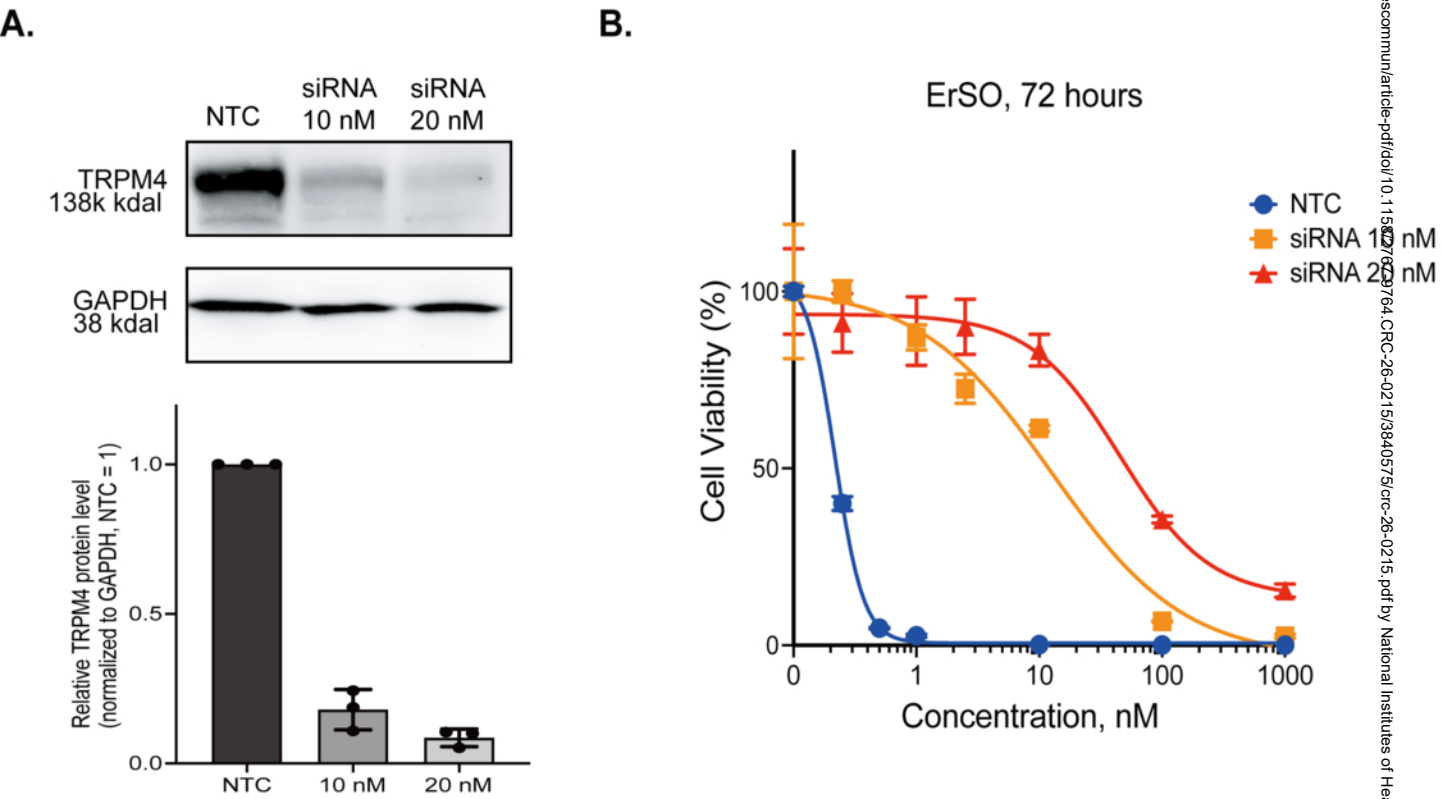
Downloaded from aacrjournals.org/cancerrescommun/article-pdf/doi/10.1158/2767-9764.CRC-26-0215/3840575/crc-26-0215.pdf by National Institutes of Health user on 31 October 2026

Figure 1



Downloaded from aacrjournals.org/cancerrescommun/article-pdf/doi/10.1158/2767-9764.CRC-26-0215/3840575/crc-26-0215.pdf by National Institutes of Health user on 31 October 2026

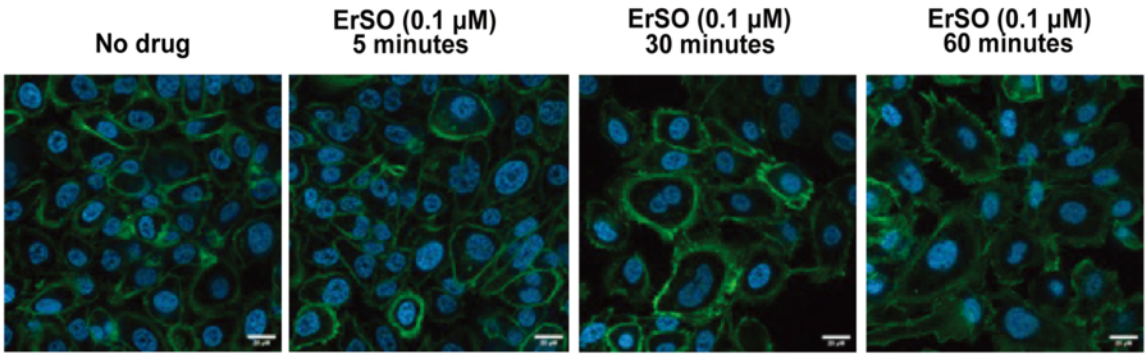
Figure 2



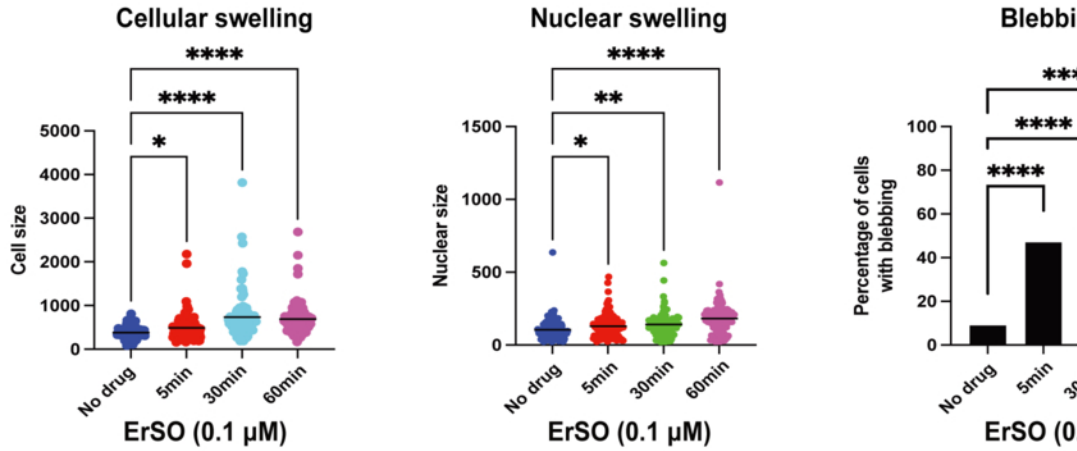
ls.org/cancerrescommun/article-pdf/doi/10.1158/2767-9764.CRC-26-0215/3840575/crc-26-0215.pdf by National Institutes of He

Figure 3

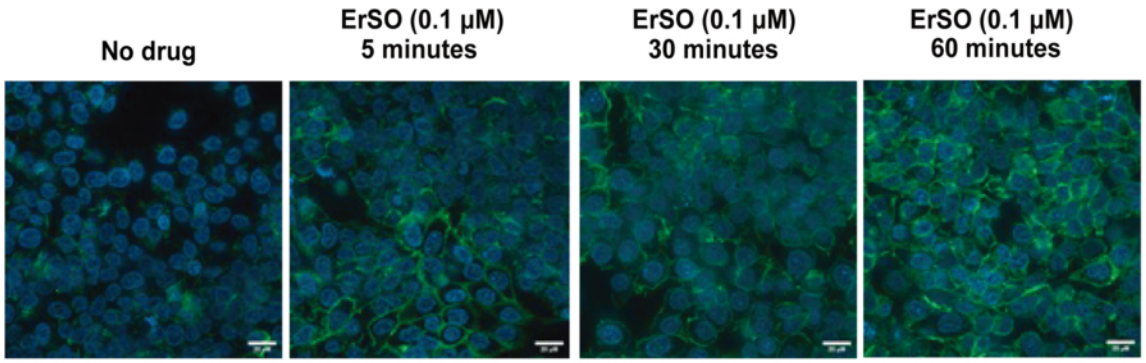
A. PC3 (high TRPM4)



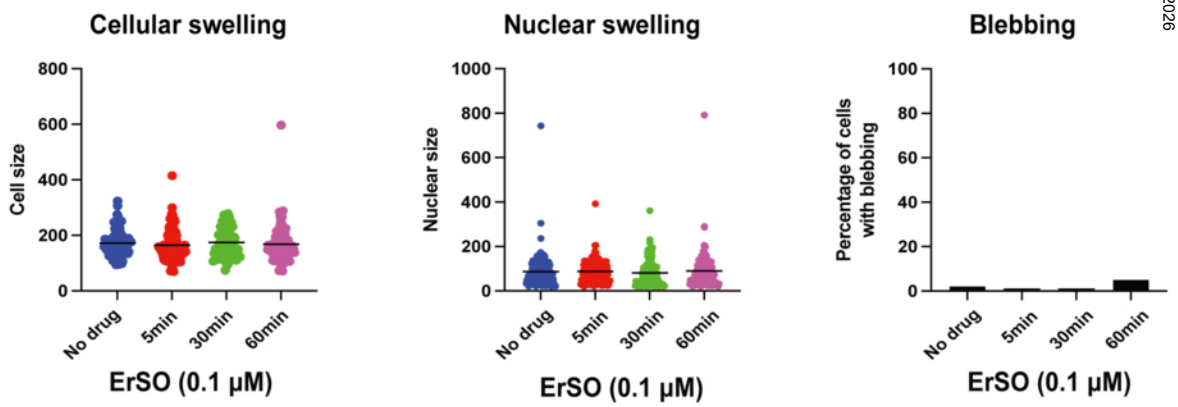
B. PC3 (high TRPM4)



C. DU145 (low TRPM4)

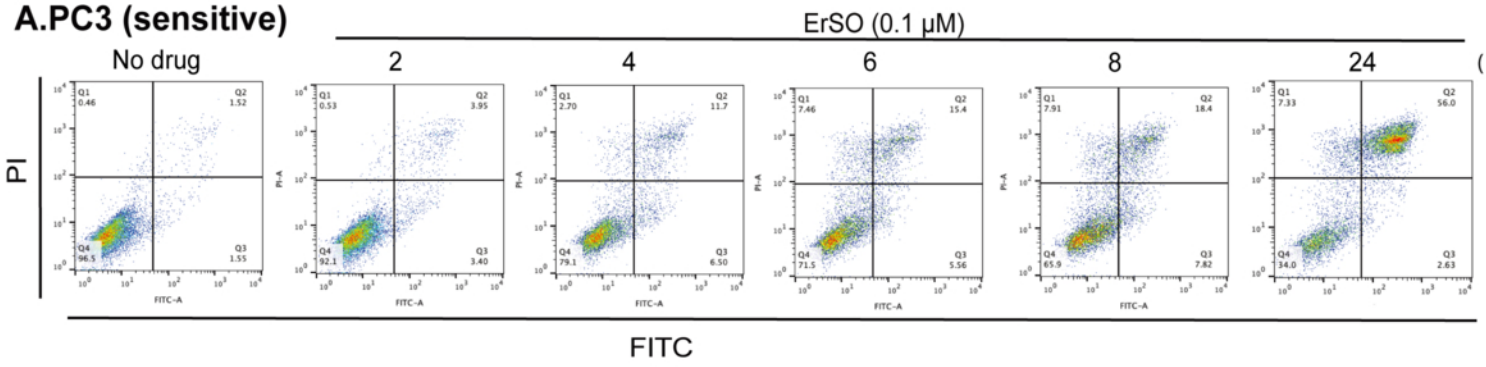


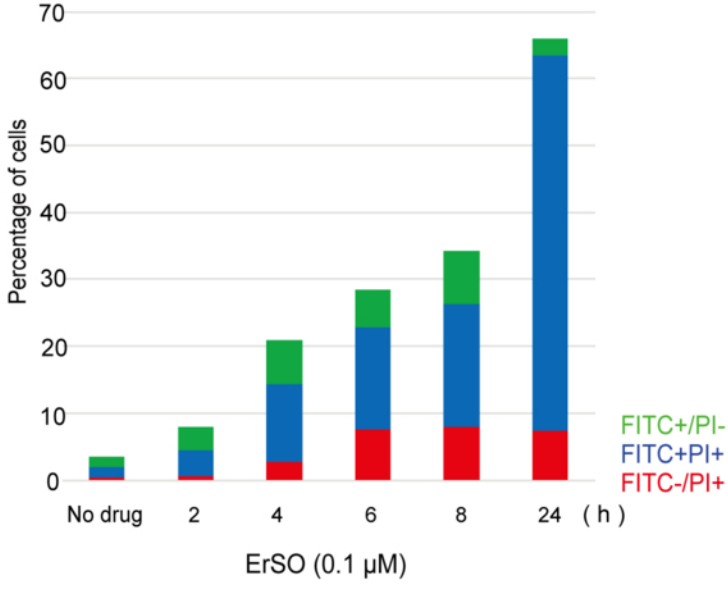
D. DU145 (low TRPM4)

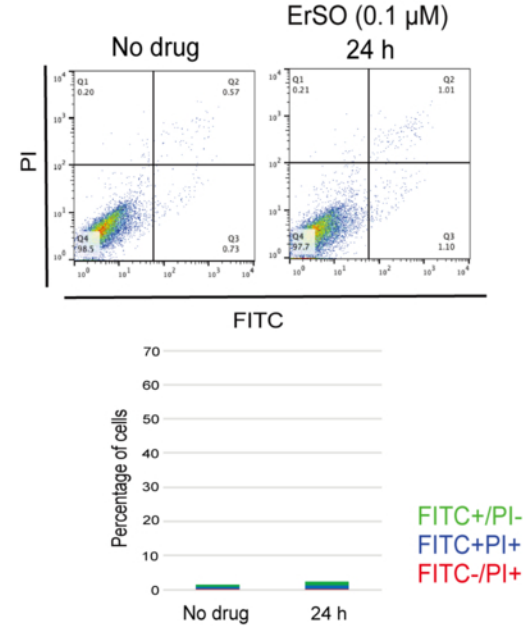


Downloaded from aacrjournals.org/cancerrescommun/article-pdf/doi/10.1158/2767-9764.CRC-26-0215/3840575/crc-26-0215.pdf by National Institutes of Health user on 31 October 2026

Figure 4

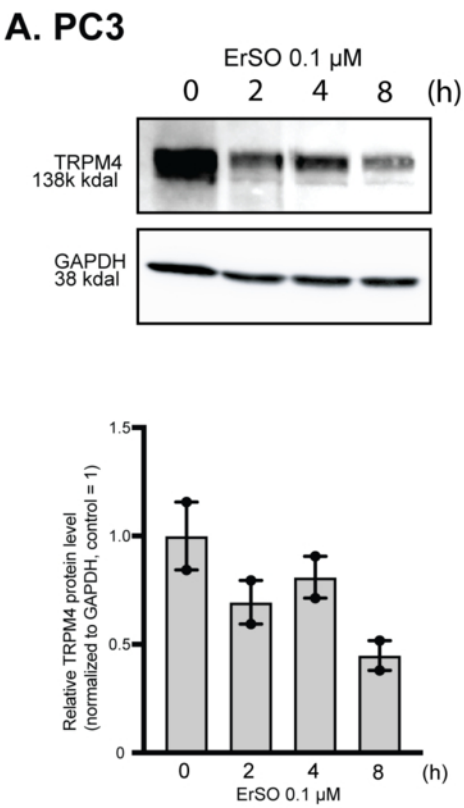


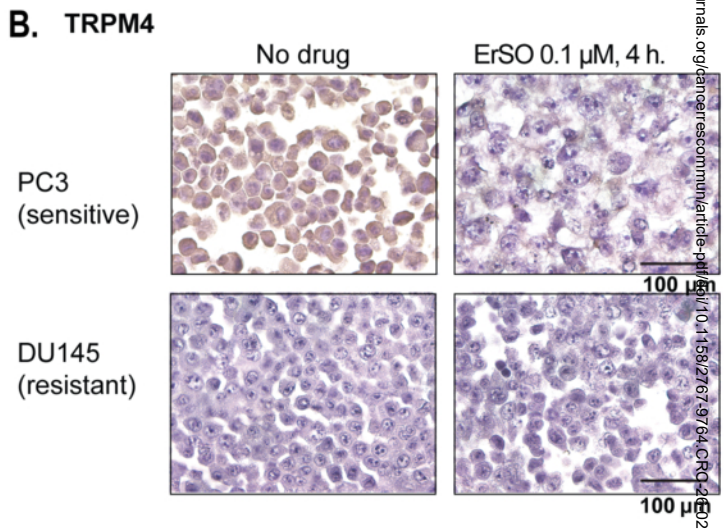


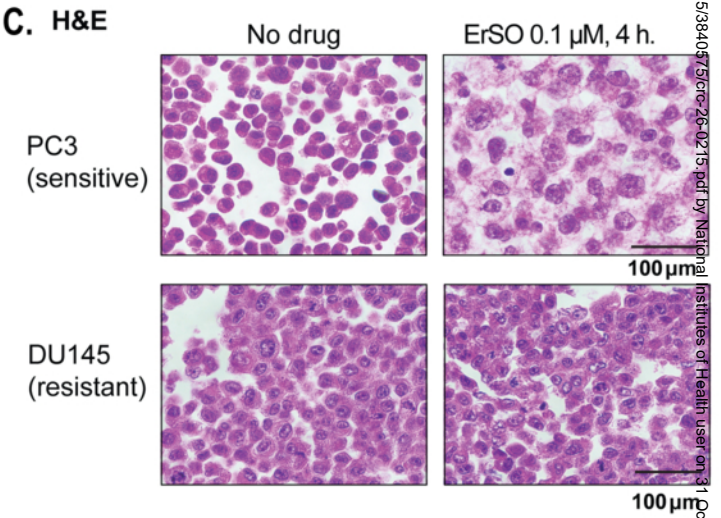


ed from aacrjournals.org/cancerrescommun/article-pdf/doi/10.1158/2767-9764.CRC-26-0215/3840575/crc-26-0215.pdf by National Institutes of Health user on 31 Octo

Figure 5

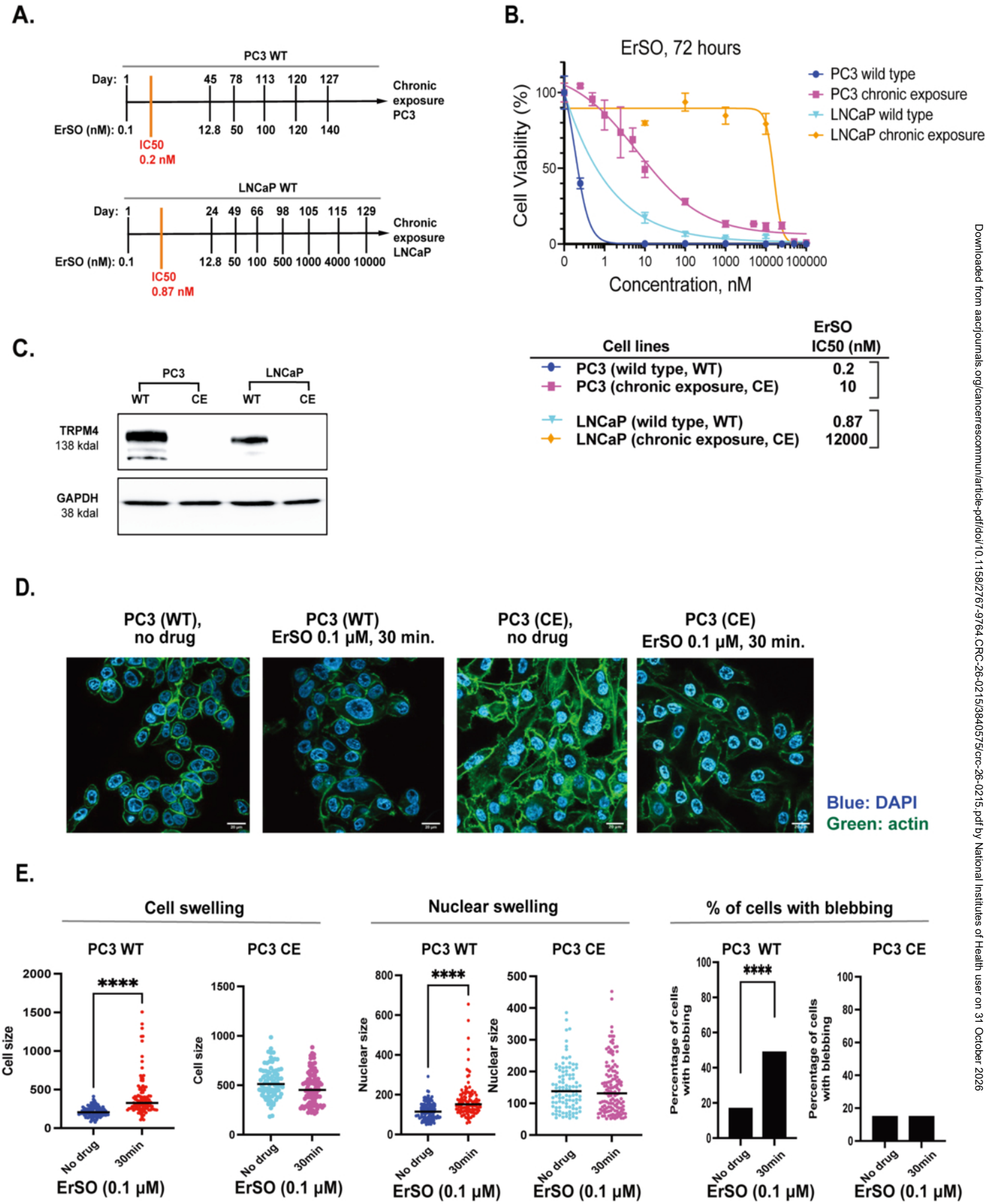






Downloaded from aacrjournals.org/cancerrescommun/article-pdf/10.1158/2767-9764.CRC-25-0215/3840575/crc-25-0215.pdf by National Institutes of Health user on 31 Oc

Figure 6



Downloaded from aacrjournals.org/cancerrescommun/article-pdf/doi/10.1158/2767-9764.CRC-26-0215/3840575/crc-26-0215.pdf by National Institutes of Health user on 31 October 2026